SIX DEGREE OF FREEDOM MORPHING AIRCRAFT DYNAMICAL MODEL

WITH AERODYNAMICS

A Thesis

by

ADAM NIKSCH

Submitted to the Office of Graduate Studies of
Texas A&M University
in partial fulfillment of the requirements for the degree of

MASTER OF SCIENCE

August 2009

Major Subject: Aerospace Engineering

SIX DEGREE OF FREEDOM MORPHING AIRCRAFT DYNAMICAL MODEL WITH AERODYNAMICS

A Thesis

by

ADAM NIKSCH

Submitted to the Office of Graduate Studies of
Texas A&M University
in partial fulfillment of the requirements for the degree of

MASTER OF SCIENCE

Approved by:

Chair of Committee,	John Valasek
Committee Members,	Thomas W. Strganac
	Leland A. Carlson
	Reza Langari
Head of Department,	Dimitris Lagoudas

August 2009

Major Subject: Aerospace Engineering

ABSTRACT

Six Degree of Freedom Morphing Aircraft Dynamical Model with Aerodynamics.

(August 2009)

Adam Niksch, B.S., Texas A&M University

Chair of Advisory Committee: Dr. John Valasek

Morphing aircraft are envisioned to have multirole capability where the ability to change shape allows for adaptation to a changing mission environment. In order to calculate the properties of many wing configurations efficiently and rapidly, a model of a morphing aircraft is needed. This paper develops an aerodynamic model and a dynamic model of a morphing flying wing aircraft. The dynamic model includes realistic aerodynamic forces, consisting of lift, drag, and pitching moment about the leading edge, calculated using a constant strength source doublet panel method. The panel method allows for the calculation of aerodynamic forces due to large scale shape changing effects. The aerodynamic model allows for asymmetric configurations in order to generate rolling and yawing moments. The dynamic model calculates state information for the morphing wing based on the aerodynamic forces from the panel method. The model allows for multiple shape changing degrees-of-freedom for the wing, including thickness, sweep, dihedral angle, and chord length. Results show the model provides a versatile and computationally efficient tool for calculating the aerodynamic forces on the morphing aircraft and using these forces to show the associated states.

NOMENCLATURE

r	Coordinate vector of any point (x,y,z)
$\mathbf{n}$	Normal vector
A	Doublet influence coefficient
B	Source influence coefficient
q	Local velocity
Q	Total Velocity
C	Aerodynamic coefficient
S	Wing Area
m	Mass
$\mathbf{v}$	Velocity vector
u	Body x-axis velocity
v	Body y-axis velocity
w	Body z-axis velocity
p	Body axis roll rate
q	Body axis pitch rate
r	Body axis yaw rate
X	Body x-axis aerodynamic force
Y	Body y-axis aerodynamic force
Z	Body z-axis aerodynamic force
T	Thrust force
G	Gravitational force
g	Acceleration due to gravity
D	Drag Force
L	Lift Force

L	Moment vector
h	Angular momentum vector
I	Inertia matrix
I_{xx}	Airplane moment of inertia about X-axis
I_{xy}	Airplane product of inertia in the XY-plane
I_{xz}	Airplane product of inertia in the XZ-plane
I_{yy}	Airplane moment of inertia about Y-axis
I_{yz}	Airplane product of inertia in the YZ-plane
I_{zz}	Airplane moment of inertia about Z-axis
L_A	Aerodynamic rolling moment
M_A	Aerodynamic pitching moment
N_A	Aerodynamic yawing moment
V	Total velocity
Greek	
α	Angle-of-attack
β	Sideslip angle
θ	Pitch attitude angle
ϕ	Roll attitude angle
ψ	Yaw attitude angle
ω	Angular velocity vector
Φ	Velocity potential
σ	Source strength
μ	Doublet strength

Subscripts

∞	Freestream condition
l	Tangential direction
m	Tangential direction
n	Normal direction
p	Pressure
F	Force
x	Body x-axis direction
y	Body y-axis direction
z	Body z-axis direction

Superscripts

N	With respect to an inertial frame
B	With respect to a body frame

Symbols

$\cdot$	Time derivative

ACKNOWLEDGMENTS

TABLE OF CONTENTS

LIST OF TABLES

LIST OF FIGURES

FIGURE   Page

CHAPTER I

INTRODUCTION

Recent interest in morphing air vehicles has been increased due to advances in smart materials and their associated electronic components. While several definitions for morphing exist, it is generally accepted that morphing refers to a large scale change in the original shape of the body. The National Aeronautics and Space Administration's (NASA) Morphing Project defines morphing as an efficient, multi-point adaptability that includes macro, micro, structural and/or fluidic approaches [1]. The Defense Advanced Research Projects Agency (DARPA) defines morphing to be a platform that is able to change its shape substantially (approximately 50 per cent or more) in order to adapt to a changing environment, making the vehicle superior in the new environment than before the change. In this paper, the authors use the DARPA definition of morphing.

There have been other attempts at calculating different aspects of a morphing air vehicle. Table I shows some of these attempts and the associated characteristics.

In Reference [2], the authors examine the aerodynamic and aeroelastic characteristics of a morphing wing. The authors use variable span method in order to allow the wing to change its shape, thereby increasing its aspect ratio and wing area, which improves overall performance at different flight conditions. Reference [3] discusses the design, development and testing of an inflatable telescopic wing that permits a change in the aspect ratio while simultaneously supporting structural wing loads. Reference [4] studies a hyper elliptic cambered span wing that is allowed to morph and creates a nonlinear, CFD based, dynamic vehicle simulation. In Reference [5],

The journal model is *IEEE Transactions on Automatic Control.*

Table I. Different Morphing Aircraft Models

Reference	Morphing Vehicle	Aerodynamics	Dynamics
[2]	Cruise Missile with Variable Span	Pressure Differencing	Aeroelastic
[3]	Inflatable Telescopic Wing	X-Foil and NACA Airfoil Data	None
[4]	Hyper-Elliptic Cambered Span Wing	CFD	Nonlinear
[5]	Airfoil	CFD	None
[6]	Morphing UAV	Aeroelastic Stability Derivatives	Aeroelastic
[7]	General Wing with Morphing Airfoils	Vortex-Lattice Method	Aeroelastic
[8]	ARES-C	Weissingers method	Longitudinal
[9]	Morphing Wing	Unsteady	Aeroelastic
[10]	Folding Wing Aircraft	None	Flexible Multibody
[11]	Morphing Airfoil	XFOIL	Actuation Dynamics
[12]	Morphing UAV/UCAV	Panel Method	None
[13]	Folding Wing Aircraft	Not Shown	ADAMS
[14]	Morphing Ellipsoid	Projected Area for Drag	Nonlinear

the authors discuss the use of a CFD model which is used to help find the optimal airfoil shape for numerous flight conditions. In Reference [6] the authors use a linear parameter-varying model to capture the aeroelastic morphing dynamics of a morphing UAV. The authors assume a variable geometry rigid body but use quasi-steady aeroelastic effects to correct the dynamic coefficients. In Reference [7], structural and aeroelastic modeling were looked into for a morphing wing. The model was able to provide actuator forces, moments, strokes, and power requirements to satisfy given vehicle performance requirements. The authors also use a vortex lattice method in order to study roll performance of the air vehicle. In Reference [15], the effects of morphing on vehicle kinematics and fuel consumption are discussed.

Reference [16] investigates the dynamics associated with large scale morphing aircraft. Specifically, the authors investigate the inertial forces and moments not apparent in the standard rigid body equations. In Reference [8], the authors examine the longitudinal dynamics of a perching aircraft concept. A generalized lifting line method is used to calculate the aerodynamic forces on the perching aircraft. Reference [9] investigates the dynamic aeroelastic stability of a morphing wing structure, specifically by investigating the migration of the wing flutter boundary in the case of a morphing aircraft. The wing is able to change span via telescoping. In Reference [10], the authors investigated the applicability of existing simulation techniques in the analysis of a non-traditional morphing aircraft design. Reference [11] attempts to optimize the shape of a morphing airfoil which will lead to low aerodynamic drag as well as low actuator energy usage.

Reference [17] discusses the application of various bio-inspired morphing concepts to unmanned aerial vehicles. The authors used a six degree-of-freedom simulation to evaluate the stability and dynamics of a morphing vehicle to various shape changes. Reference [18] focuses on a morphing airfoil concept. The focus is on the physical

shape change of the airfoil modeled by a space/time transform parameterization. Reference [12] studies the effects of variable sweep, wing area, and aspect ratio on low speed performance. Specifically, range and endurance are addressed for speeds of up to Mach 0.8. Reference [13] describes the development of a simulation tool to study the time domain, in-flight behavior of aircraft morphing mechanisms. In Reference [19], the authors attempt to develop a design scheme aimed at minimizing structural load and actuator power on a span morphing aircraft.

In Reference [14], the authors modeled a wing as an ellipsoid that was assumed to have constant volume. The chord thickness dimensions were allowed to change freely, while the span dimension was determined by the constant volume assumption. The equations of motion were derived, with time varying inertias to account for the shape change effect. In reference [20], the authors used a similar model to the one in Reference [14]. The authors used this model in order to test a control methodology for morphing which based on a combination of reinforcement learning and adaptive dynamic inversion control. During this test, the model simultaneously tracks a specified trajectory and changes shape autonomously, based on flight conditions, over the course of the trajectory.

This research expands upon previous research done in Reference [14]. The scope of this research includes the inviscid,incompressible flow regime. Thus, only the linear region of the aerodynamics is considered. A computational model of a morphing aircraft is developed which includes accurate aerodynamics for the inviscid, incompressible flow regime and the ability to handle both small scale and large scale shape changes. Some of the issues which arise from creating this model are creating an accurate yet computationally efficient aerodynamic model and combining the aerodynamic model with a dynamical model in order to calculate state information. The main objective of this research is to create a computational model for a morphing air

vehicle which includes:

- Accurate aerodynamics for inviscid, incompressible flow

- Nonlinear flight dynamics

- Multiple shape changing degrees-of-freedom

- Run in a MATLAB environment

- The ability to be accessed by other subroutines for future research

The first step in this research is to create an aerodynamic model of a morphing airfoil section. This is accomplished by creating a numerical model of the airfoil section using a doublet panel method with multiple shape changing parameters. Next, an aerodynamic model for a morphing aircraft is developed. The morphing aircraft is chosen to be a flying wing type of aircraft. This is also accomplished by using a constant strength source-doublet panel method, with more shape changing parameters added. Once the aerodynamic model of the morphing aircraft has been developed, a dynamical model of the morphing aircraft is developed using nonlinear six degree-of-freedom aircraft equations of motion in order to record time histories of the aircraft state information. The final stage in this research validates the aerodynamic and dynamic models of the morphing aircraft using known experimental data as well as other proven numerical methods. This thesis shows the computational model developed is versatile and allows for the manipulation of multiple shape changing degrees-of-freedom. This is important because this model will be used in future research to help determine optimal shapes for a wing at a given flight condition. The model also is able to combine nonlinear dynamics with accurate aerodynamic forces within the scope of this research, where the aerodynamic forces a function of the wing geometry.

CHAPTER II

AIRFOIL MODEL REPRESENTATION

To calculate the aerodynamic properties of many different airfoils in a short period of time, or as a single airfoil changes shape, a numerical model of the airfoil is developed. A constant strength doublet panel method is used to model the aerodynamics of the airfoil. The main assumption is that the flow is incompressible, otherwise a much more complex model is necessary. This assumption is valid because current interests lie in the realm of micro air vehicles, which fly at speeds less than Mach 0.3. Other assumptions are that both the upper and lower surfaces of the airfoil are pinned at the leading and trailing edge rendering the structural moment at these points to be zero. These boundary conditions become important in later sections in the calculation of M_y and σ_{xx}. One final assumption is that the flow is inviscid. Thus the model is only valid for the linear range of angle-of-attack.

The flexibility of this type of model allows the reinforcement learning algorithm developed to manipulate three degrees of freedom, one flight condition parameter, and one material parameter. The degrees of freedom, flight condition parameter, and material parameter are:

- Airfoil thickness

- Camber

- Chord

- Airfoil angle-of-attack

Despite this versatility there are some limitations to the model. Since the model uses a panel method to calculate the aerodynamics, it is very sensitive to the grid,

or location of the panels, and the number of panels created. The grid must be a sinusoidal spaced grid in the x direction, which puts more points at the trailing edge of the airfoil. This type of grid is necessary because many aerodynamic changes occur near the trailing edge. If the number of panels were to decrease, the accuracy of the model would also decrease. However, as the number of panels generated is increased, the computational time of the model increases as well. Thus, a balance is needed between accuracy and computational time. This balance can be achieved by finding a set number of panels for which any increase from that number of panels yields a minimal accuracy increase. For example, assume 50 panels are chosen initially. If the number of panels were changed to 100 and the accuracy of the model increased by 10 per cent, this increase in the number of panels would be deemed necessary. If the number of panels were changed from 100 to 150 and the accuracy of the model increased by less than 1 per cent, then this increase in the number of panels would be deemed unescessary, and 100 panels is chosen as the correct number of panels to use.

The airfoil model uses a sinusoidal spacing for the grid. This allows for more panels to be placed at the leading and trailing edges of the airfoil. This type of grid is similar to cosine spacing. By using this type of grid, the overall number of panels required is less and the computational time required is reduced. The control points are placed at the center of each of the panels. The total number of panels chosen is 200, with 100 on the upper surface and 100 on the lower surface of the airfoil. The outputs of this model are lift, drag, pitching moment about the leading edge, stress, and strain.

A. Airfoil Model Development

The aerodynamics of the airfoil is modeled by a constant strength doublet panel method. For each panel consider first the velocities in the local panel coordinate system

$$u_p = \frac{\mu}{2\pi}\left[\frac{z}{(x-x_1)^2 + z^2} - \frac{z}{(x-x_2)^2 + z^2}\right] \tag{2.1}$$

$$w_p = \frac{\mu}{2\pi}\left[\frac{x-x_1}{(x-x_1)^2 + z^2} - \frac{x-x_2}{(x-x_2)^2 + z^2}\right] \tag{2.2}$$

Since these equations require panel coordinates, a transformation from the global coordinate system to the local panel coordinate system must be made. The following equation represents the coordinate transformation used[21]

$$\begin{pmatrix} x \\ z \end{pmatrix}_p = \begin{pmatrix} \cos(\theta_i) & -\sin(\theta_i) \\ \sin(\theta_i) & \cos(\theta_i) \end{pmatrix} \begin{pmatrix} x - x_0 \\ z - z_0 \end{pmatrix} \tag{2.3}$$

The panel method is based on the no penetration condition, which states that the flow cannot cross the solid boundary of the airfoil, thus the velocity normal to the surface is 0 in the global coordinate system. Eq. 2.4 transforms the velocities from Eqs. 2.1 and 2.2 into the global coordinate system.[21]

$$\begin{pmatrix} u \\ w \end{pmatrix} = \begin{pmatrix} \cos(\theta_i) & \sin(\theta_i) \\ -\sin(\theta_i) & \cos(\theta_i) \end{pmatrix} \begin{pmatrix} u_p \\ w_p \end{pmatrix} \tag{2.4}$$

Now it is possible to solve for the doublet strengths using Eqs. 2.1-2.4. These doublet strengths are then used to find the tangential velocities at each point. Once the tangential velocities are calculated, the pressure coefficient can be calculated using Bernoulli's equation which, when modified, produces Eq. 2.5 [22].

$$C_p = 1 - \frac{u^2 + w^2}{V_\infty^2} \tag{2.5}$$

The pressure coefficient can be broken up into normal and axial forces using simple integration. These forces can also be further broken up into lift and drag using simple trigonometry.[22]

$$C_n = \frac{1}{c} \int_0^c \left(C_{p_{lower}} - C_{p_{upper}} \right) dx \tag{2.6}$$

$$C_a = \frac{1}{c} \int_0^c \left(C_{p_{upper}} \frac{dy_{upper}}{dx} - C_{p_{lower}} \frac{dy_{lower}}{dx} \right) dx \tag{2.7}$$

$$C_l = C_n \cos(\alpha) - C_a \sin(\alpha) \tag{2.8}$$

$$C_d = C_n \sin(\alpha) + C_a \cos(\alpha) \tag{2.9}$$

Once the pressure distribution has been calculated, the pressures found are assumed to be the loads on the airfoil, which are needed to apply basic beam theory. The pressure distribution is approximated using a curve fit function so that the stress values can be easily calculated. One disadvantage of using a curve fit function is the resulting curve is not the exact pressure distribution and thus an error will be present. In order to decrease this error, the order of the polynomial fitted to the pressure distribution should be increased. As with the panel accuracy case, too large of an increase in the order of the polynomial will result in increased compuational time as well as a minimal accuracy increase. Once again, a balance is necessary in order to achieve a high accuracy with low compuational time. The balance between accuracy and compuational time is found by using the same method as when finding the correct number of panels to be used. The stress values for both the upper and lower surfaces of the airfoil are calculated using Eqs. 2.10 and 2.11.[23] Eq. 2.10 is the basic boundary value problem from Euler-Bernoulli Beam Theory. Once Eq. 2.10 is solved, Eq. 2.11 is used to calculate the stress at any point on the surface.

$$\frac{dM}{dx} = P \tag{2.10}$$

$$\sigma_{xx} = \frac{-M \cdot y}{I_{zz}} \tag{2.11}$$

CHAPTER III

AIRFOIL MODEL VALIDATION AND VERIFICATION

This section validates the mathematics and physics of the airfoil model, and then verifies that it accurately represents the desired airfoil. For the validation, two representative airfoils were examined for correct pressure and lift profile characteristics corresponding to a conventional airfoil. For verification, wind tunnel data from Ref. [24] was compared to the data generated by the doublet panel model.

A. Aerodynamic Validation

The first airfoil modeled was a NACA 0012, representing the class of symmetric airfoils. The constant strength doublet panel method was applied producing the pressure distribution illustrated in Figure 1. The angle-of-attack is held at 0°, so there should be zero calculated lift on the airfoil. The pressure distribution is shown in the following figure:
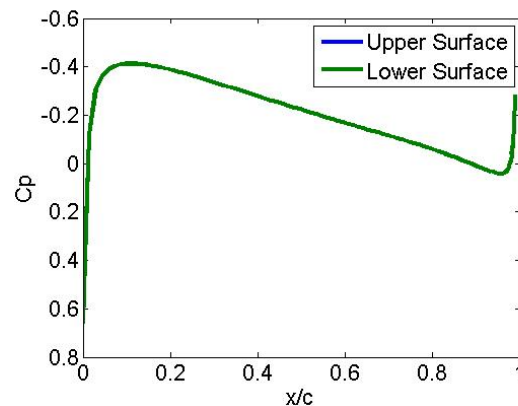

Fig. 1. Pressure Distribution Across a NACA 0012 Airfoil

An asymmetric airfoil was also modeled. The representative airfoil chosen was the NACA 4412. Figure 2 shows the pressure distribution produced by the constant strength doublet panel code for a NACA 4412 held at 0°.
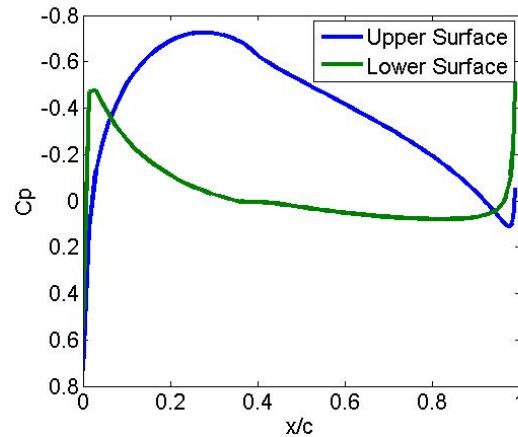

Fig. 2. Pressure Distribution Across a NACA 4412 Aifoil.

Calculating the lift and drag based on Figure 1 and Figure 2 result in no lift on the symmetric airfoil and positive lift on the asymmetric airfoil. These results are reasonably accurate with respect to the physics involved, and indicate that the airfoil model produces reasonably correct aerodynamics. However, as can be seen from Figure 1 and Figure 2, there are problems associated with the trailing edge in each of these airfoils. This discrepancy is due to the singularity present at the trailing edge and is a known issue with doublet panel methods. The singularity at the trailing edge is a source of error for constant strength doublet panel methods that must be taken into account when analyzing results. The trailing edge discrepancy can be eliminated by adding a constant strength source to the doublet panel method. There is also some error that arises when calculating the lift and drag coefficients because they are calculated by numerically integrating the resultant pressure distribution.

The numerical error associated with integrating the pressure distribution tends to make this method less accurate than other methods. However, since the pressure distribution is needed in order to calculate the stress and strain on the airfoil, it was decided to calculate lift and drag by integration.

B. Structural Validation

Structural analysis of the NACA 0012 and NACA 4412 based on the doublet panel model was also conducted. The stress distribution for both the NACA 0012 and NACA 4412 are illustrated in Figure 3 and Figure 4, respectively. Both assume sea level conditions and a speed of about 100 m/s.
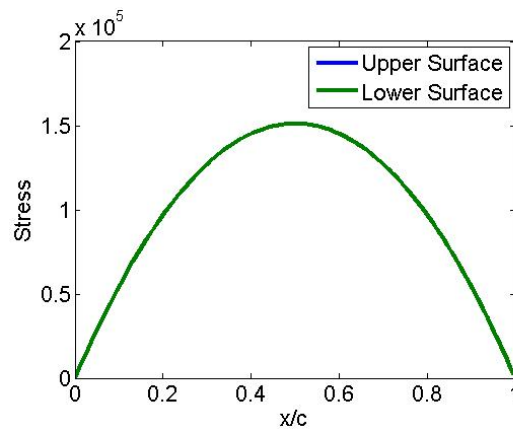

Fig. 3. Stres Distribution of a NACA 0012

These figures show how the stress varies with position along both the upper and the lower surface of the airfoils. The stress values appear to be low and require further investigation. However, the general shape of stress distribution is to be expected. There is greater stress toward the center of the airfoil where there is greater bending moment. Also, the distribution for the symmetric airfoil shows that the stress is
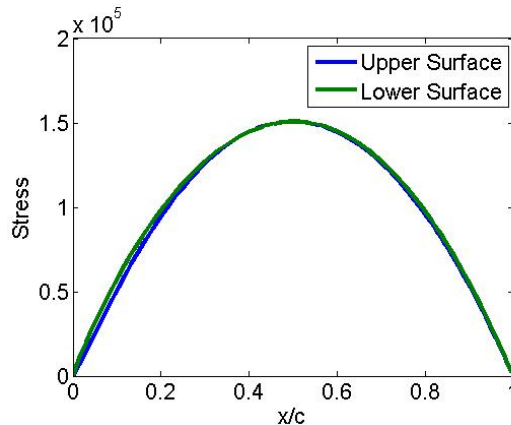
Fig. 4. Stress Distribution of a NACA 4412

equal for both surfaces adhering to the characteristic symmetry of the airfoil, whereas there is a slight difference in the asymmetric airfoil stress distribution. The top and bottom surfaces are not mirrors of each other, which thus results in different stress distributions.

C. Verification

Several sets of airfoil data were compared to verify the accuracy of the model within the scope of this research. For brevity, only one set of data is presented here. The lift curve produced by the model for the NACA 0012 is compared to wind tunnel data from Ref. [24] and is depicted in Figure 5. Note the wind tunnel data which the model is compared to includes viscous effects and has a Reynold's number of six million.

Since the doublet panel model is limited the linear range of the airfoil angle-of-attack, the angles-of-attack only ranged from -5 to 5 degrees. When compared to data from Ref. [24], there were some discrepancies, but they are considered mild
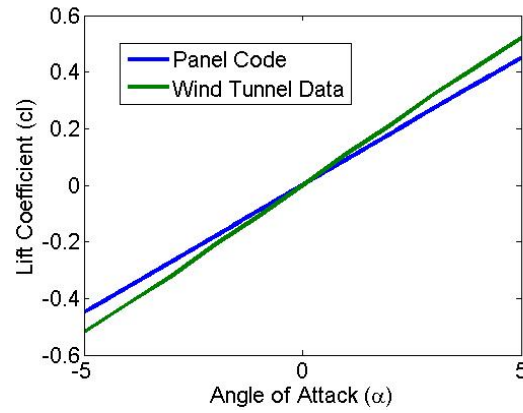
Fig. 5. Lift Curve Slope for a NACA 0012

and acceptable for this problem. Some of these discrepancies arise from the singularity inherent in this modeling method, while others come from the limitations and assumptions needed to apply the method.

CHAPTER IV

FULL AERODYNAMIC MODEL REPRESENTATION

To calculate the aerodynamic properties of many wing configurations efficiently and rapidly, a numerical model of the wing aerodynamics is developed. A constant strength doublet-source panel method is used to model the aerodynamics of the wing. This method was chosen over other CFD methods due to the success using a panel method in predicting the aerodynamic effects on a morphing airfoil. By using a source-doublet method, the effect of thickness is captured, which is often an effect neglected by other types of panel methods. The main assumption is that the flow is incompressible; otherwise a much more complex model is necessary. This assumption is valid because current interests lie in the realm of air vehicles which fly at speeds less than Mach 0.3. One other assumption is that the flow is inviscid. Thus, the model is only valid for the linear range of angle-of-attack. A method provided by DATCOM is used to estimate the profile drag.

The versatility of this type of model allows the author's reinforcement learning algorithm developed in Reference [25] to manipulate multiple morphing degrees of freedom and flight condition parameters. The morphing degrees of freedom and flight condition parameters are:

- wing root airfoil thickness

- left wing tip airfoil thickness

- right wing tip airfoil thickness

- wing root airfoil camber

- left wing tip airfoil camber

- right wing tip airfoil camber

- wing root airfoil location of maximum camber

- left wing tip airfoil location of maximum camber

- right wing tip airfoil location of maximum camber

- wing span

- aspect ratio

- leading edge sweep angle

- dihedral angle

- taper ratio

- twist

Yet, given this versatility, there are some limitations to the model. Since the model uses a panel method to determine the aerodynamics, it is very sensitive to the grid size, location of the panels, and the number of panels created. The grid uses cosine spacing for both chordwise and spanwise panels. By utilizing cosine spacing, more panels are placed near the leading and trailing edges of the wing as well as at the root and tip. This type of grid is necessary because many aerodynamic changes occur near the leading and trailing edges as well as at the tips of the wing. As the number of panels decrease, the accuracy of the model also decreases. However, as the number of panels is increased, the computational time of the model increases as well. Thus, a balance is needed between accuracy and computational time. This balance is achieved by defining a set number of panels for which any increase from that number of panels yields a minimal increase in accuracy. For example, if the number of panels

were doubled and the accuracy of the model increased by 10 per cent, this increase in the number of panels would be deemed acceptable. However, if this set of panels were increased by 50 per cent and the accuracy increased by less than 1 per cent, then this increase in the number of panels would be deemed unnecessary.

Also, the model has a limitation on the different types of airfoil sections which can be used. Only NACA 4-Digit Series airfoils are considered because there are explicit equations which easily describe the upper surface and the lower surface geometries. These equations have defined thickness and camber variables, which makes them easy to examine and optimize to achieve the best possible wing shape.

The aerodynamic model uses 130 chordwise panels, with 65 on the upper surface and 65 on the lower surface, and 25 spanwise panels for the half-span. Thus, 3250 total panels are used to model the half-span. The aerodynamic model does not assume a plane of symmetry, so each half of the wing is modeled separately. The control points are placed at the center of each panel. The outputs of the aerodynamic model are lift, drag, pitching moment about the apex, rolling moment, and yawing moment. The lateral and directional outputs are only shown if the morphing wing is asymmetric.

A.   Aerodynamic Modeling

The wing is modeled using a constant strength doublet-source panel method. In order to obtain the equations for aerodynamic forces on a wing, basic potential flow theory is used. Equation 1 is the basic equation of potential flow theory [21].

$$\nabla^2 \Phi = 0 \tag{4.1}$$

Equation 4.1 satisfies the inviscid and incompressible flow assumptions to the general conservation equations. Using Green's identity, a solution to Equation 4.1 is

formed with a sum of source σ and doublet μ distributions along the boundary, SB.

$$\Phi = -\frac{1}{4\pi} \int\limits_{SB} \left[\sigma \left(\frac{1}{r} \right) - \mu \mathbf{n} \cdot \nabla \left(\frac{1}{r} \right) \right] dS + \Phi_\infty \tag{4.2}$$

Assuming the wake convects at the trailing edge of the wing as a set of by thin doublets, Equation 4.2 may be rewritten as

$$\Phi = \frac{1}{4\pi} \int\limits_{Body+Wake} \mu \mathbf{n} \cdot \nabla \left(\frac{1}{r} \right) dS - \frac{1}{4\pi} \int\limits_{Body} \sigma \left(\frac{1}{r} \right) dS + \Phi_\infty \tag{4.3}$$

The boundary condition for Equation 4.1 is the no penetration condition, which requires the normal velocity of the flow at the surface to equal to zero. This boundary condition must be specified by either a direct or indirect formulation. The direct formulation forces the normal velocity component to be zero and is defined to be the Neumann problem. The indirect formulation specifies a value for the potential function on the boundary and, by doing so, the zero normal flow condition is indirectly satisfied. This method is defined to be the Dirichlet problem. The morphing wing model uses the Dirichlet problem to enforce the zero normal flow boundary condition. Using the Dirichlet boundary condition, the potential must be specified at all points on the boundary. If a point is placed inside the surface, the inner potential, Φ_i, is defined by the singularity distributions along the surface.

$$\Phi_i = \frac{1}{4\pi} \int\limits_{Body+Wake} \mu \frac{\partial}{\partial \mathbf{n}} \left(\frac{1}{r} \right) dS - \frac{1}{4\pi} \int\limits_{Body} \sigma \left(\frac{1}{r} \right) dS + \Phi_\infty \tag{4.4}$$

These integrals become singular as r approaches zero. In order to evaluate the integrals near this point, the no penetration boundary condition must be enforced. In order to enforce this boundary condition, Φ_i is set to a constant value. If the direct formulation is used, it may be shown that Φ_i is a constant. Since Φ_i is a constant, Equation 4.4 is equal to a constant as well. The constant value of Φ_i is chosen to be

Φ_∞. Thus, Equation 4.4 is reduced to a simpler form.

$$\frac{1}{4\pi} \int\limits_{Body+Wake} \mu \frac{\partial}{\partial \mathbf{n}} \left(\frac{1}{r}\right) dS - \frac{1}{4\pi} \int\limits_{Body} \sigma \left(\frac{1}{r}\right) dS = 0 \tag{4.5}$$

Next, one reduces these integral equations to a set of linear algebraic equations. Let the system be divided into N panels for the surface and N_w panels for the wake, as shown in Figure 6 [21]. The boundary condition is specified at a collocation point, which for the Dirichlet boundary condition is inside the body and at the center of the panel. Equation 4.5 is rewritten for N collocation points for N panels. The integrands shown below only depend on the geometry of the respective panel, and thus can be evaluated.
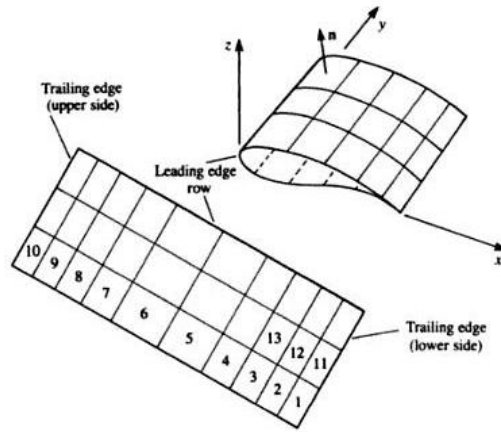

Fig. 6. Paneling on a Wing

$$\sum_{k=1}^{N} \frac{1}{4\pi} \int\limits_{BodyPanel} \mu \mathbf{n} \cdot \nabla \left(\frac{1}{r}\right) dS + \sum_{l=1}^{N} \frac{1}{4\pi} \int\limits_{WakePanel} \mu \mathbf{n} \cdot \nabla \left(\frac{1}{r}\right) dS$$

$$- \sum_{k=1}^{N} \frac{1}{4\pi} \int\limits_{BodyPanel} \sigma \left(\frac{1}{r}\right) dS = 0 \tag{4.6}$$

Since the singularity elements, μ and σ, of each panel influence every other panel on the body, Equation 4.6 may be rewritten for each collocation point inside the body. Note that the variables preceding the singularity elements are the respective integrals evaluated for a particular panel and the respective collocation point. Thus,

$$\sum_{k=1}^{N} A_k \mu_k + \sum_{l=1}^{N} A_l \mu_l - \sum_{k=1}^{N} B_k \sigma_K = 0 \tag{4.7}$$

In order to eliminate the wake strength from Equation 4.7, a new relationship is introduced. The Kutta condition states there is no circulation at the trailing edge of a wing section. By using the Kutta condtion, one will find the doublet strength of the wake panel is equivalent to the difference between the trailing edge panels on the upper surface and the lower surface. Figure 7 shows this relationship [21]. By exploiting
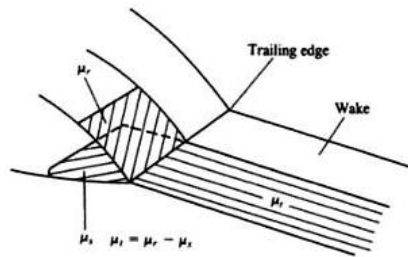

Fig. 7. Relationship of the Wake Panels to the Trailing Edge Panels

this relationship, the wake contribution may be eliminated from Equation 4.7 by substitution at the trailing edge panels only. Since the source strengths are known, Equation 4.7 reduces to a set of N equations with N unknown doublet strengths which

may be solved by matrix inversion.

$$
\begin{pmatrix} a_{11} & \cdots & a_{1N} \\ \vdots & \ddots & \vdots \\ a_{N1} & \cdots & a_{NN} \end{pmatrix} \begin{pmatrix} \mu_1 \\ \vdots \\ \mu_N \end{pmatrix} = - \begin{pmatrix} b_{11} & \cdots & b_{1N} \\ \vdots & \ddots & \vdots \\ b_{N1} & \cdots & b_{NN} \end{pmatrix} \begin{pmatrix} \sigma_1 \\ \vdots \\ \sigma_N \end{pmatrix}
\tag{4.8}
$$

Once the doublet strengths are found, it is possible to find the aerodynamic forces acting on each panel. The first step is to determine the tangential and normal perturbation velocity components for each of the panels. Note that the partial derivatives are taken with respect to the local panel coordinate system, which is shown in Figure 8 [21].

$$
q_l = -\frac{\partial \mu}{\partial l}, q_m = -\frac{\partial \mu}{\partial m}, q_n = -\sigma
\tag{4.9}
$$

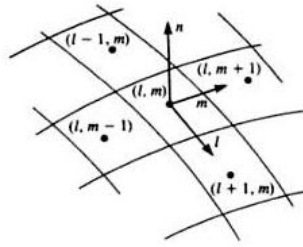With these velocities , the total velocity of each panel may be computed.

Fig. 8. Panel Coordinate System

$$
Q_k = (Q_{\infty l}, Q_{\infty m}, Q_{\infty n})_k + (q_l, q_m, q_n)_k
\tag{4.10}
$$

Using the velocities at each panel, the pressure coefficient at each panel is found

using a modified form of Bernoulli's Equation.

$$C_{p_k} = 1 - \frac{Q_k^2}{Q_\infty^2} \tag{4.11}$$

Once the pressure coefficient has been determined, the non-dimensional aerodynamic forces are calculated for each panel. The total aerodynamic forces are found by summing the contributions from each panel.

$$\Delta C_{F_k} = -\frac{C_{p_k} \Delta S}{S} \cdot \mathbf{n}_k \tag{4.12}$$

Reference [26] shows a DATCOM method for calculating the value of parasite drag, C_{D_0}, based on the wing area and the equivalent parasite area.

$$C_{D_0} = \frac{f}{S} \tag{4.13}$$

The equivalent parasite area is related to the wetted area of the morphing wing aircraft as

$$\log_{10} f = a + b \log_{10} S_{wet} \tag{4.14}$$

The terms a and b are correlation coefficients related to the equivalent skin friction of the aircraft. The equivalent skin friction coefficient is estimated by using data from similar aircraft.

The Oswald efficiency factor may be expressed as a function of the aspect ratio of the wing and is valid if the leading edge sweep angle of the wing is less than 30°. Equation 4.15 provides the Oswald efficiency factor, which was developed empirically in Reference [27].

$$e = 1.78(1 - 0.045AR^{0.68}) - 0.64 \tag{4.15}$$

Once the Oswald efficiency factor has been determined, an expression for the total drag acting on the morphing wing can be constructed. Equation 4.16 provides this

relationship.

$$C_D = C_{D_0} + \frac{C_L^2}{\pi e AR} \qquad (4.16)$$

B.   Model Grid

One important aspect of this model is the ability to generate a grid which is easy to manipulate and easily allows for many morphing degrees of freedom. In order to accomplish this, the first step is to represent the airfoil sections that allow for camber and thickness to change and be suitable for flight conditions that are within the incompressible regime. There are multiple ways to accomplish this. One way is to create a table of known airfoil coordinates for look up whenever a reconfiguration occurs. The advantages of this type of representation are the wide variety of airfoils available for selection and the ease with which to transition from one type of airfoil to another. However, the major disadvantage of a table with multiple airfoil sections is not being able to have direct control over the thickness and camber of the airfoil. For this model, being able to have direct, quick control for a change in thickness and camber is vital. Therefore, the approach which was chosen is to use a set of airfoils for which there were equations that describe the upper and lower geometries of the airfoil section as a function of a thickness and camber. The class of airfoils chosen are the NACA 4-Digit series airfoils. Herein, only 4-Digit airfoils can be chosen. These airfoils have blunt leading edges with either thick or thin airfoil sections, which makes them ideal for subsonic speeds.

The method of spacing used to place the panels on the wing is also an important aspect of generating a grid. For this particular model, cosine spacing is utilized for both chordwise and spanwise paneling. The cosine spacing method is defined by the following equation [28].

$$x_{v_i} = \frac{c(y)}{2}\left(1 - \cos\left(\frac{i\pi}{N+1}\right)\right)$$
$$i = 1 : N$$

(4.17)

By using cosine spacing in the chordwise direction, more panels are placed near the leading edges and trailing edges of the wing. Cosine spacing in the spanwise direction places more panels at the span stations which are near the tips of the wing. Figures 9, 10, and 11 show the effect of utilizing cosine spacing in both the spanwise and chordwise directions as well as some of the different shapes which the aerodynamic model is able to model. As can be seen from the figures, the four corner points on the wing have the most number of panels.
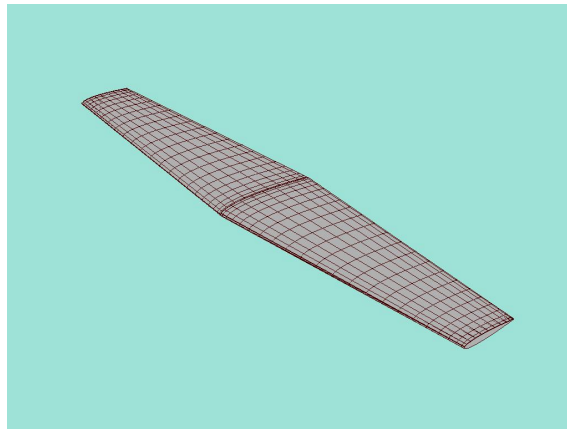

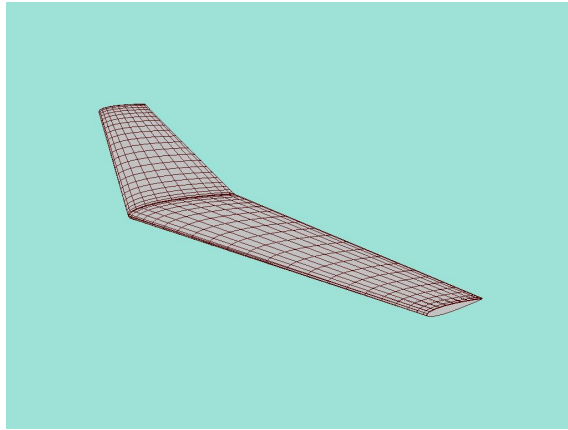Fig. 9. Tapered Wing with Cosine Spacing
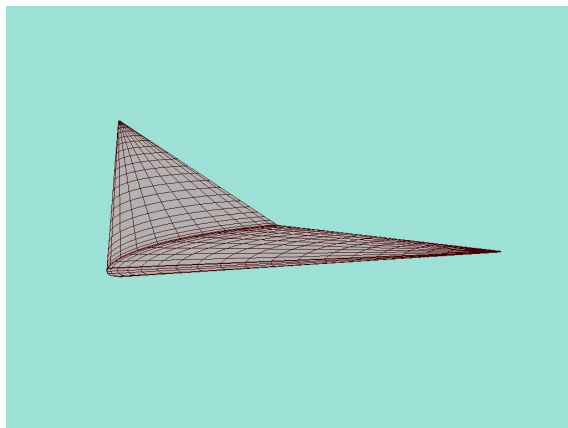
Fig. 10. Swept Wing with Cosine Spacing

Fig. 11. Delta Wing with Cosine Spacing

CHAPTER V

AERODYNAMIC MODEL VALIDATION AND VERIFICATION

This chapter presents the results of the aerodynamic model for the morphing wing and verifies it accurately represents the shape represented. The aerodynamic model is compared, for two cases, to a model which was developed by Dr. Leland Carlson at Texas A&M University called TRANS3DNS. TRANS3DNS solves the three-dimensional extended transonic small perturbation equations and can allow for wing sweep, taper, twist, and different airfoil sections.

A.   Validation

This section validates the aerodynamic model for the morphing wing using two example cases. The first example is a rectangular wing planform with a NACA 2212 airfoil section. This example is used confirm the wing model compares with known cases. The second example uses a wing with a 15° leading edge sweep angle, a NACA 2412 airfoil section, and a taper ratio of 0.7. This example is used to test shape changes and verify the accuracy of the model during these shape changes.

1.   Example 1: Rectangular Wing Planform

This example tests the aerodynamic model using a rectangular wing planform with a NACA 0012 airfoil section. The aerodynamic model produces the lift, drag, and moment data illustrated in Figures 12, 13, and 14, respectively.

Figure 13 shows the variation of the induced drag for the morphing wing in this example. The drag polar is plotted as a function of the lift coefficient.

Figure 14 shows the variation of the pitching moment about the leading edge of the wing root with respect to the angle-of-attack.
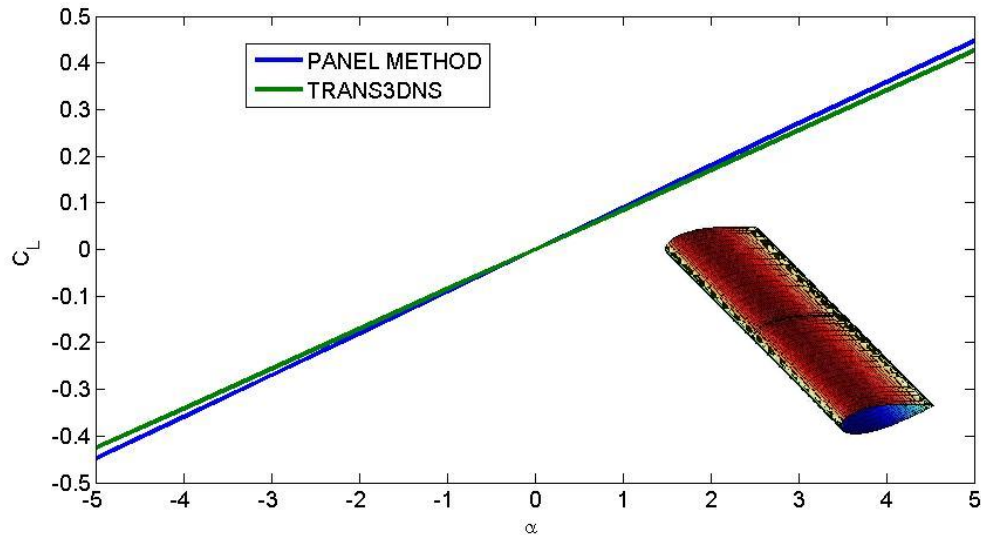
Fig. 12. Lift Curve for Example #1

These results are accurate with respect to the physics involved and indicate the aerodynamic model produces reasonably accurate aerodynamics on a basic wing shape. However, due to the assumptions made and the method in which the aerodynamic forces are calculated, there is some error present when this data is compared with TRANS3DNS. Since TRANS3DNS uses a small perturbation method to calculate the aerodynamic forces, TRANS3DNS will have discrepancies when compared to any panel method. TRANS3DNS also does not take into account the thickness of the airfoil section, whereas the aerodynamic model does consider thickness. As the thickness of an airfoil tends to increase, the lift curve slope will increase as well. As a result, the panel method shows an increased value in lift curve slope.
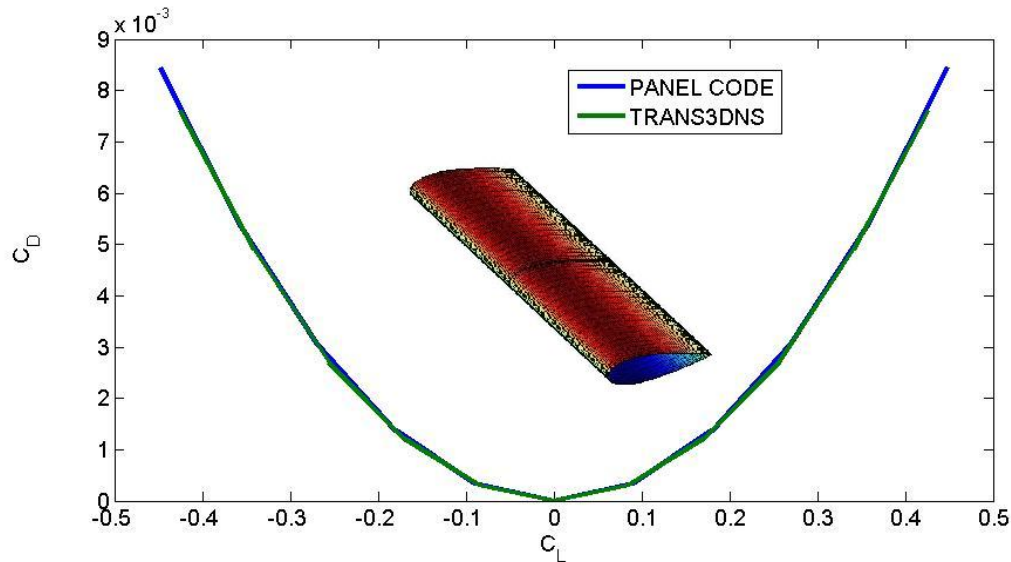
Fig. 13. Drag Polar for Example #1

2. Example 2: Nonrectangular Wing Planform

This example tests the aerodynamic model using a wing with a 15° leading edge sweep angle, a taper ratio of 0.7, and a NACA 2412 airfoil section. The aerodynamic model produces the lift, drag, and moment data in Figures 15,16, and 17, respectively.

A drag polar is constructed using the aerodynamic model. The induced drag for the morphing wing, as a function of lift coefficient, is shown in Figure 16.

Figure 17 shows the variation of the pitching moment about the leading edge of the wing root with respect to the angle-of-attack.

Again, these results are reasonably accurate with respect to the physics involved. By adding camber to the airfoil section, the lift curve slope is shifted. Adding a leading edge sweep angle causes the lift curve slope to decrease when compared with an unswept configuration. By adding taper to the wing, there is less lift produced at the wing tips, thus lowering the overall lift generated from the wing. As in the
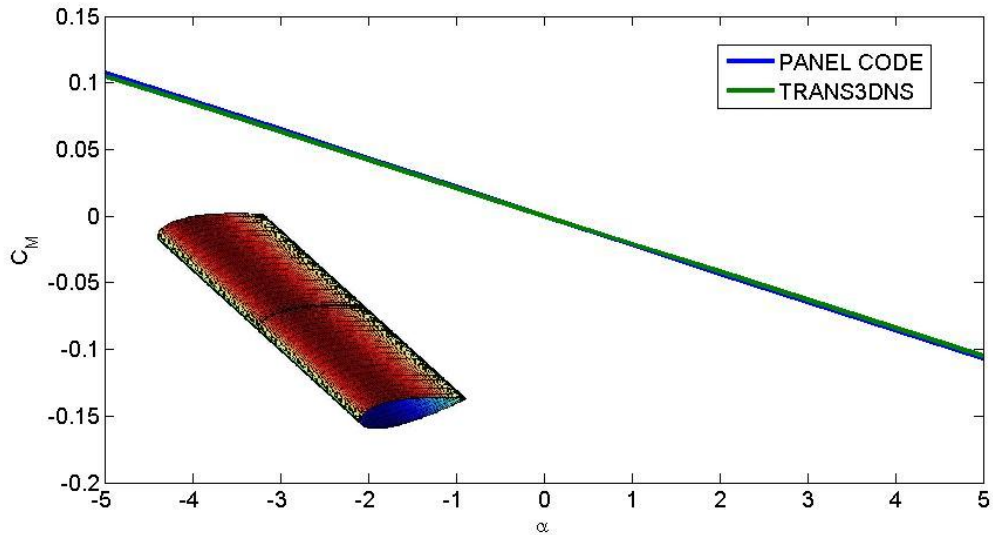
Fig. 14. Leading Edge Moment Curve for Example #1

first example, there are sources of error within this method. A source of error for the more complex shape is the aerodynamic code uses a first order sweep correction method. Another source of error is from the thickness effect, as in the previous example. The effect of airfoil thickness appears to effect the lift coefficient at zero angle of attack. While slightly larger than the previous example, these errors have been deemed acceptable for this research.

B. Verification

This section is used to verify the the aerodynamic model against a known physical case. Theory states that as the aspect ratio of a wing increases, the value of the lift curve slope should asymptotically approach $2\pi_i$. The aerodynamic model is applied, producing the plot shown in Figure 18.

The figure shows that the lift curve slope is approaching a value close to 2π.
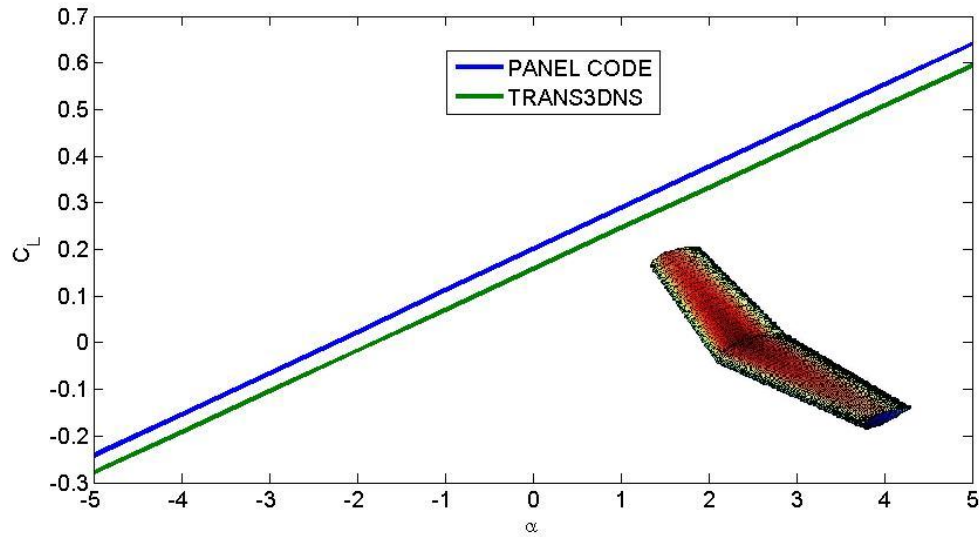
Fig. 15. Lift Curve for Example #2

However, because of the effect of airfoil thickness, it is possible for the panel method to approach a value which is slightly higher than 2π. If the effects of viscosity were modeled, then the lift curve slope would be lowered and would settle to a value very near 2π. For the purpose of this research however, the aspect ratio will not exceed 12 nor be lower than three. Therefore, any errors which are present in this case have been deemed acceptable.
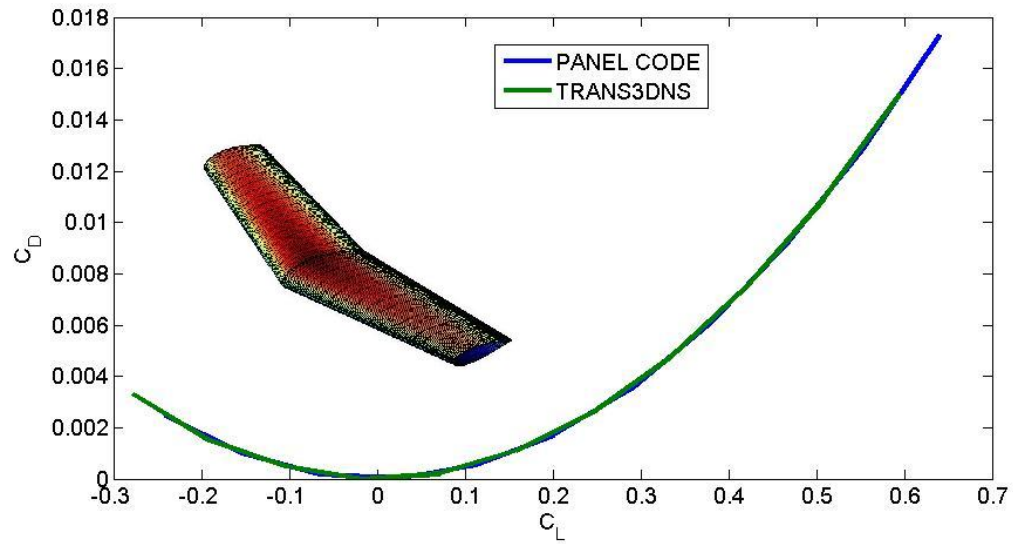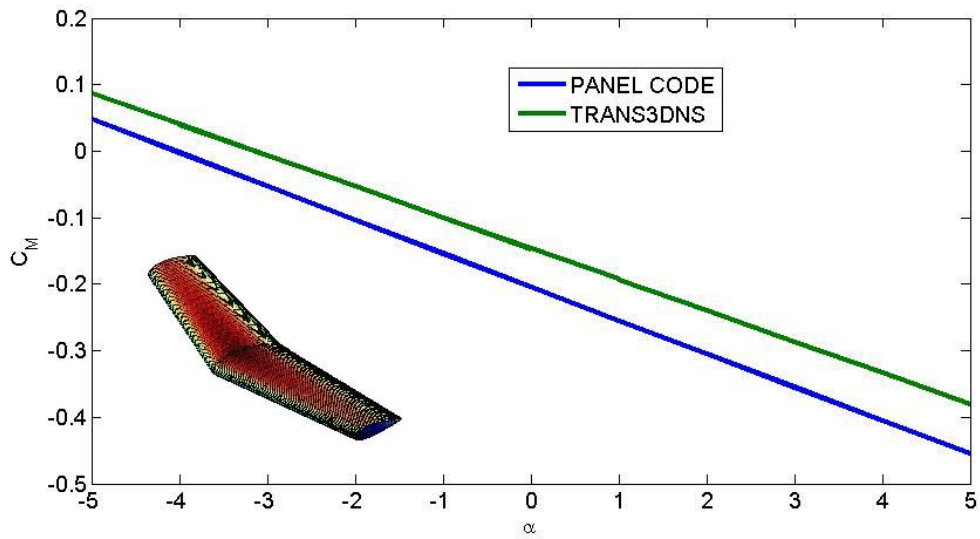
Fig. 16. Drag Polar for Example #2

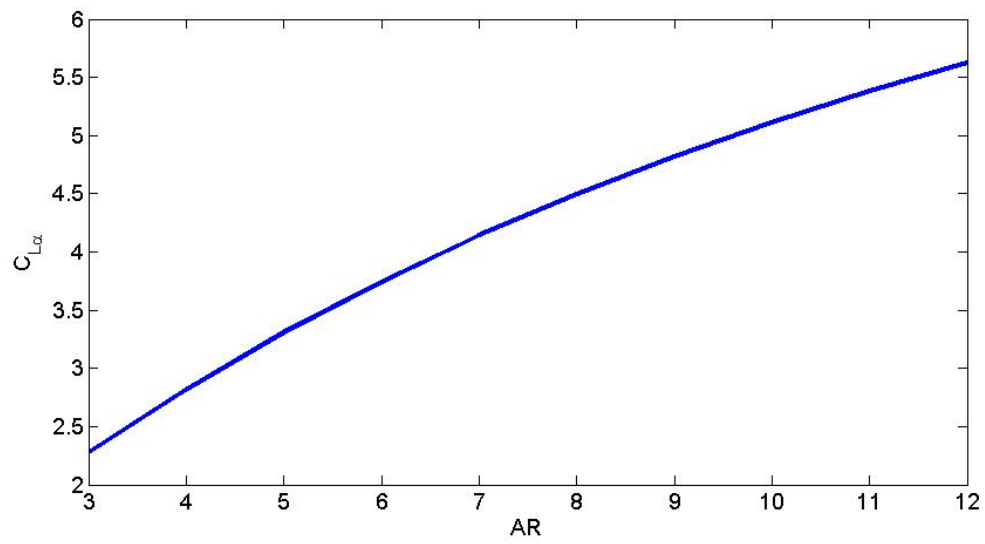Fig. 17. Leading Edge Moment Curve for Example #2

Fig. 18. Lift Curve Slope Variation with Aspect Ratio

CHAPTER VI

DYNAMIC MODEL DEVELOPMENT

Starting with Newton's Second Law, $\mathbf{F} = m\dot{\mathbf{v}}^N$, the translational equations of motion for the morphing wing may be developed. The body axis system can be seen in Figure 19. Note that the same convention is used in the following derivation as by Roskam [29]. Consider a velocity vector $\mathbf{v}$ and an angular velocity vector ω expressed in the body axis system of the morphing wing.
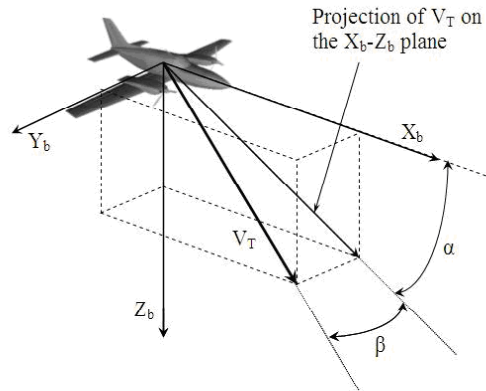

Fig. 19. Aircraft Body Axis System

$$\mathbf{v} = \begin{pmatrix} u \\ v \\ w \end{pmatrix} \tag{6.1}$$

$$\omega = \begin{pmatrix} p \\ q \\ r \end{pmatrix} \tag{6.2}$$

Taking an inertial derivative of the velocity vector with respect to time yields

$$\dot{\mathbf{v}}^N = \dot{\mathbf{v}}^B + \omega \times \mathbf{v} = \begin{bmatrix} \dot{u} + qw - rv \\ \dot{v} + ru - pw \\ \dot{w} + pv - qu \end{bmatrix} \tag{6.3}$$

The forces acting on the morphing wing consist of gravitational, propulsive, and aerodynamic forces. The gravitational forces can be easily calculated using simple trigonometry. The propulsive force acting on the morphing wing is assumed to be constant. The only remaining forces are the aerodynamic forces, which are calculated using the constant strength source-doublet panel method mentioned in Chapter IV.The forces acting on the morphing wing are

$$\mathbf{F} = \begin{bmatrix} X + T_x + G_x \\ Y + T_y + G_y \\ Z + T_z + G_z \end{bmatrix}$$

$$= \begin{bmatrix} -mg\sin(\theta) - D\cos(\alpha)\cos(\beta) + L\sin(\alpha)\cos(\beta) + T \\ mg\sin(\phi)\cos(\theta) + D\cos(\alpha)\sin(\beta) - L\sin(\alpha)\sin(\beta) \\ mg\cos(\phi)\cos(\theta) - D\sin(\alpha) - L\cos(\alpha) \end{bmatrix} \tag{6.4}$$

Substituting Equation 6.3 and Equation 6.4 into Newton's Second Law, the translational equations of motion are obtained. These translational equations of motion are

$$m(\dot{u} + qw - rv) = -mg\sin(\theta) - D\cos(\alpha)\cos(\beta) + L\sin(\alpha)\cos(\beta) + T \tag{6.5}$$

$$m(\dot{v} + ru - pw) = mg\sin(\phi)\cos(\theta) + D\cos(\alpha)\sin(\beta) - L\sin(\alpha)\sin(\beta) \tag{6.6}$$

$$m(\dot{w} + pv - qu) = mg\cos(\phi)\cos(\theta) - D\sin(\alpha) - L\cos(\alpha) \tag{6.7}$$

Using Euler's Equations, $\mathbf{L} = \dot{\mathbf{h}}^N$, one may obtain a relationship between the rotational motion and the moments acting on the morphing wing. Consider an angular momentum vector $\mathbf{h}$, defined as

$$\mathbf{h} = \mathbf{I}\omega \tag{6.8}$$

The inertia matrix, $\mathbf{I}$, may be written as

$$\mathbf{I} = \begin{pmatrix} I_{xx} & -I_{xy} & -I_{xz} \\ -I_{xy} & I_{yy} & -I_{yz} \\ -I_{xz} & -I_{yz} & I_{zz} \end{pmatrix} \tag{6.9}$$

These moments of inertia are functions of the configuration of the morphing wing. These inertias are time varying and represent the morphing wing due to the shape changes that occur during flight. Taking the time derivative of the angular momentum vector, the following relationship is obtained.

$$
\begin{aligned}
\dot{\mathbf{h}}^N &= \mathbf{I}\dot{\omega}^B + \dot{\mathbf{I}}^B\omega + \omega \times \mathbf{I}\omega \\
&= \begin{bmatrix}
I_{xx}\dot{p} - I_{xy}\dot{q} - I_{xz}\dot{r} + \dot{I}_{xx}p - \dot{I}_{xy}q - \dot{I}_{xz}r + p\left(-I_{xz}q + I_{xy}r\right) \\
+q\left(-I_{yz}q - I_{yy}r\right) + r\left(I_{zz}q + I_{yz}r\right) \\
I_{xy}\dot{p} - I_{yy}\dot{q} - I_{yz}\dot{r} + \dot{I}_{xy}p - \dot{I}_{yy}q - \dot{I}_{yz}r + p\left(I_{xx}r + I_{xz}p\right) \\
+q\left(-I_{xy}r + I_{yz}p\right) + r\left(-I_{xz}r - I_{zz}p\right) \\
I_{xz}\dot{p} - I_{yz}\dot{q} - I_{zz}\dot{r} + \dot{I}_{xz}p - \dot{I}_{yz}q - \dot{I}_{zz}r + p\left(-I_{xy}p - I_{xx}q\right) \\
+q\left(I_{yy}p + I_{xy}q\right) + r\left(-I_{yz}p + I_{xz}q\right)
\end{bmatrix}
\end{aligned} \tag{6.10}
$$

The moments that act on the morphing wing are due to the aerodynamic forces and the propulsive forces. The moments caused by the aerodynamic forces are calculated from the panel method mentioned in Chapter IV. It is assumed for the purpose of this research that the thrust line is parallel to the body x-axis and acts at the center of gravity location, thus not producing a moment. The moments acting on the morphing

wing are

$$\mathbf{L} = \begin{bmatrix} L_A \\ M_A \\ N_A \end{bmatrix} \tag{6.11}$$

By substituting Equation 6.10 and Equation 6.11 into Euler's Equations, the rotational equations of motion for the morphing wing are

$$I_{xx}\dot{p} - I_{xy}\dot{q} - I_{xz}\dot{r} + \dot{I}_{xx}p - \dot{I}_{xy}q - \dot{I}_{xz}r + p\left(-I_{xz}q + I_{xy}r\right)$$
$$+q\left(-I_{yz}q - I_{yy}r\right) + r\left(I_{zz}q + I_{yz}r\right) = L_A \tag{6.12}$$

$$I_{xy}\dot{p} - I_{yy}\dot{q} - I_{yz}\dot{r} + \dot{I}_{xy}p - \dot{I}_{yy}q - \dot{I}_{yz}r + p\left(I_{xx}r + I_{xz}p\right)$$
$$+q\left(-I_{xy}r + I_{yz}p\right) + r\left(-I_{xz}r - I_{zz}p\right) = M_A \tag{6.13}$$

$$I_{xz}\dot{p} - I_{yz}\dot{q} - I_{zz}\dot{r} + \dot{I}_{xz}p - \dot{I}_{yz}q - \dot{I}_{zz}r + p\left(-I_{xy}p - I_{xx}q\right)$$
$$+q\left(I_{yy}p + I_{xy}q\right) + r\left(-I_{yz}p + I_{xz}q\right) = N_A \tag{6.14}$$

The other states which need to be considered are the angle-of-attack and the side-slip angle, since the aerodynamic forces are directly dependent on them. From geometry, the relationship between angle-of-attack, side-slip angle, and the respective body axis velocities can be expressed as

$$\tan\left(\alpha\right) = \frac{w}{u} \tag{6.15}$$

$$\tan\left(\beta\right) = \frac{v}{u} \tag{6.16}$$

Differentiating Equation 6.15 and Equation 6.16 with respect to time yields

$$\dot{\alpha} = \frac{1}{V}\left(\dot{w}\cos\left(\alpha\right) - \dot{u}\sin\left(\alpha\right)\right) \tag{6.17}$$

$$\dot{\beta} = \frac{1}{V}\left(\dot{v}\cos\left(\beta\right) - \dot{u}\sin\left(\beta\right)\right) \tag{6.18}$$

CHAPTER VII

DYNAMIC MODEL RESULTS

This section presents the results of the dynamic model for the morphing wing. For the first example, the aircraft does not perform any shape changing. This is done in order to observe the natural movement of the aircraft. In the second example, the aircraft starts with an initial shape and performs two shape changes during the specified time frame. The initial conditions used in both examples are the same and are listed in Table II. Note that the initial conditions for the angle-of-attack and sideslip angle states are found by using Equations 6.15 and 6.16.

A. Example 1: No Shape Changing

In this example, the morphing wing does not perform any shape changes. The fixed shape which is being observed for this example is listed below.

- NACA 0012 Airfoil Section

- Unswept

- No Dihedral

- Root Chord Length of 1.667 ft

- Tip Chord Length of 1.667 ft

- Wing Span of 10 ft

By using only one shape in this example, it is possible to observe the natural behavior of this particular configuration. This configuration will also serve as the starting point for the next example.

Table II. Initial Conditions

	Example 1	Example 2	Example 3	Example 4	Example 5
$u(ft/sec)$	50	50	50	50	50
$v(ft/sec)$	0	0	0	0	7
$w(ft/sec)$	20	0	0	0	0
$\phi(deg)$	0	0	0	0	0
$\theta(deg)$	0	10	0	0	0
$\psi(deg)$	0	0	0	0	0
$p(deg/sec)$	0	0	0	5	0
$q(deg/sec)$	0	0	0	0	0
$r(deg/sec)$	0	0	0	0	0.5
$\alpha(deg)$	21.8	0	0	0	0
$\beta(deg)$	0	0	0	0	7.97

Figure 20 shows the longitudinal state information for the morphing wing at this shape configuration. The lateral and directional state information is not shown here because these states are at a zero value for all time. The w velocity component, q, and angle-of-attack are each approaching and eventually reach a zero value. The angle-of-attack state indicates the trim point the aircraft settles at without any control devices is the zero lift configuration. By having q reach a zero value, this shows the pitch attitude angle is approaching a steady state value as well, which is $-90°$. The aircraft reaches this configuration Since the w velocity component reaches a zero value, this suggests that the velocity vector is aligning with the body x-axis. Figure 21 shows the time history of the u velocity component. This plot shows that the velocity vector is indeed aligning with the body x-axis, since this component of velocity increases until the drag force can no longer be overcome.

B.   Example 2: Longitudinal Motion with Shape Changes

In this example, the morphing aircraft will begin with the shape from the first example and performs a shape change at a time of 20 seconds. Only longitudinal motion is considered in this example. The shape changes are presented in Figure 22.

Figure 23 shows the time history of the states for the morphing aircraft. During the first time period, the aircraft appears to once again settle at a trim point in which there is no lift. However, once the shape changes to include camber and twist, the aircraft finds another trim point which to settle at, which is at an angle-of-attack of $6.07°$. At this angle of attack, the aerodynamic pitching moment generated is eliminated and positive lift is maintained on the aircraft. By adding the twist, the aircraft was able to go from the pitch attitude angle of $-90°$ in the previous example to a new pitch attitude of $-16.5°$. As in the first example, q eventually approaches
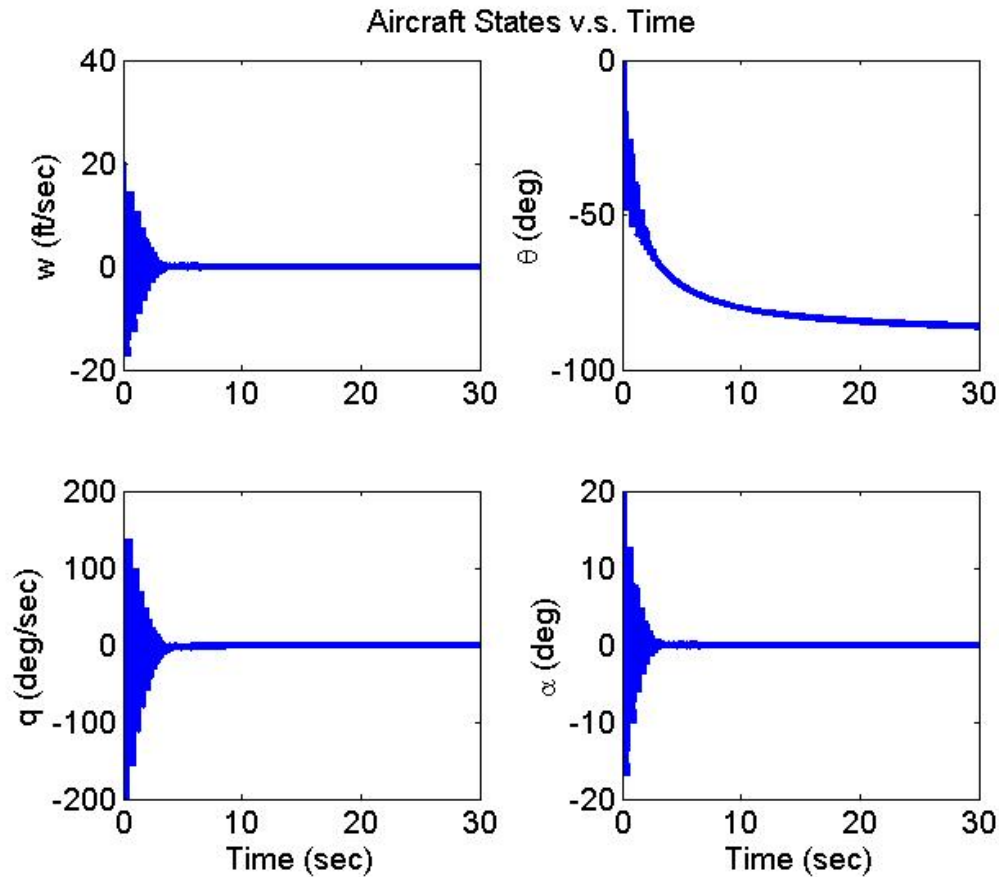
Fig. 20. Morphing Aircraft States for Example 1

zero. The w velocity component is nonzero during the phase of flight where the morphing wing has camber and twist.

Figure 24 shows the time history of the u velocity component. During the time period in which the morphing aircraft has camber and twist, u does begin to settle at a constant value. The velocity of the aircraft accelerates during the first phase of flight due to gravitational forces. When camber and twist are added, the aircraft is able to maintain a constant velocity much lower than in the previous example.
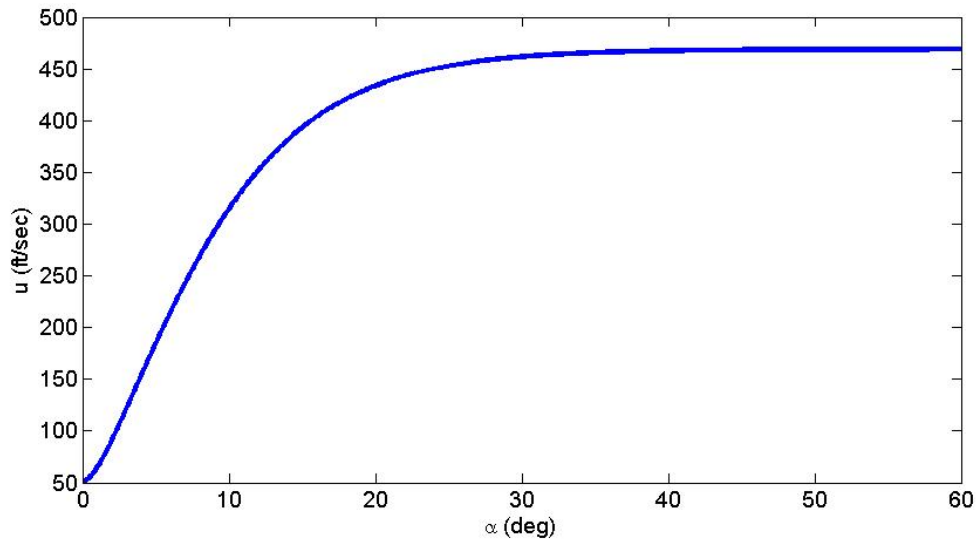
Fig. 21. Time History of u for Example 1

C.   Example 3: Longitudinal Motion with Immediate Shape Changes

In this example, the morphing aircraft will perform shape changes during the beginning portion of flight and will begin with the shape from Example 1. This example uses a different shape than the previous example and is used to show the model can handle shape changes at any point in time. The shape changes are presented in Figure 25.

Figure 26 shows the time history of the states for the morphing aircraft. Since the shape change occurs at the beginning of flight, the aircraft is able to establish positive lift while the pitching moment is slowly reduced in magnitude. The result is a slow sinusoidal type motion which resembles the phugoid mode of an aircraft. This motion is very lightly damped, though all states do eventually settle to constant values at a much later value of time. The pitch attitude angle settles at a positive value in this example and the pitch rate goes to zero. The angle-of-attack settles at
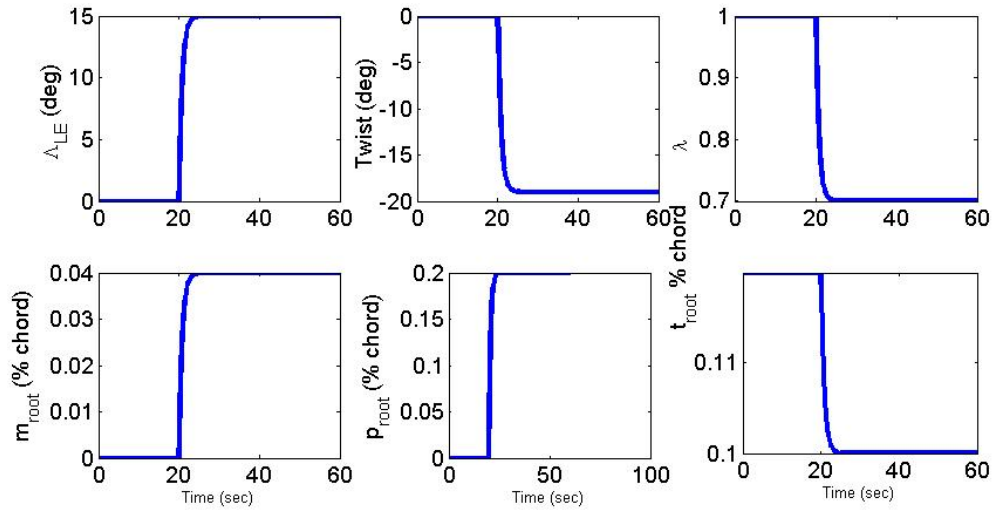
Fig. 22. Time History of Morphing Aircraft Shape for Example 2

a nonzero value which negates the aerodynamic pitching moment.

Figure 27 shows the time history of the u velocity component. The airspeed of the aircraft also follows the lightly damped, sinusoidal motion the pitch attitude angle experiences. The airspeed does eventually settle to a constant value as well, which is lower in magnitude than the first example.

D.   Example 4: Lateral/Directional Motion with Immediate Shape Changes

In this example, the morphing aircraft will begin with the shape from the first example and will immediately perform a shape change. Only lateral/directional motion is considered in this example. The shape changes are presented in Figure 28.

Figure 29 shows the time history of the states of the morphing aircraft. The roll and yaw Euler angles change slowly, due to the rapid changes in the angular velocities. The angular velocities change rapidly because the left and right airfoil sections of the
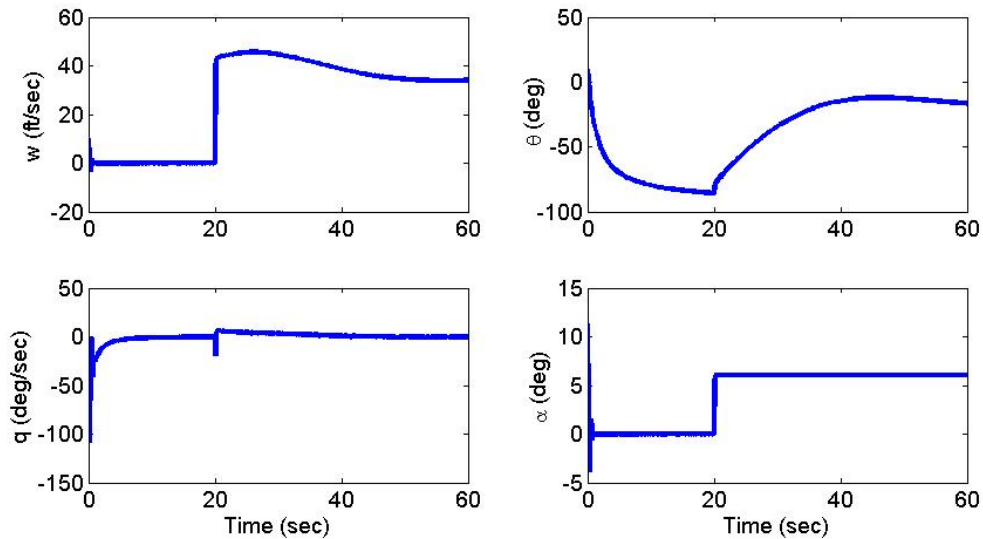
Fig. 23. Morphing Aircraft States for Example 2

morphing wing are changing in order to balance the moments acting on the aircraft. Thickness changes were used for yawing motion and camber changes were used for rolling motion. However, there is some coupling which occurs between the rolling and yawing motions. This is the source of the rapid changes in the angular velocity. The side-slip angle on the aircraft slowly increases to a nonzero value.

E.   Example 5: Lateral/Directional Motion with Delayed Shape Changes

In this example, the morphing aircraft will begin with the shape from the first example and performs a shape change at a time of 15 seconds. Only lateral/directional motion is considered in this example. The shape changes are presented in Figure 30.

Figure 31 shows the time history of the states of the morphing aircraft. The roll and yaw Euler angles begin to increase in magnitude due to a steady increase in magnitude by the angular velocity rates. Once the shape change occurs, the angular
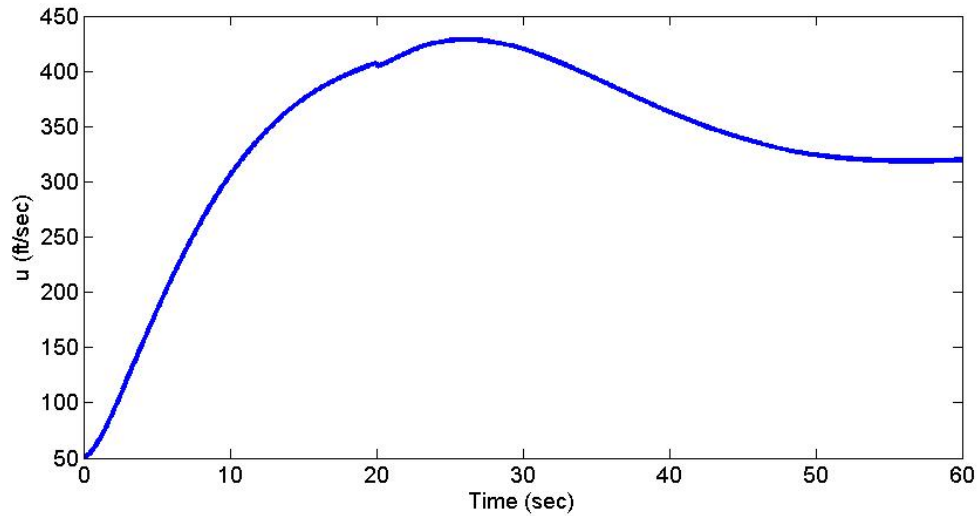
Fig. 24. Time History of u for Example 2

velocity rates begin to damp out. The damping of the roll motion is not quite as good as in the previous example, but the damping in the yawing motion is significantly improved over the previous case. This allows the yaw attitude angle to settle to a constant nonzero value. The sideslip angle decreases in magnitude before the shape change and then appears to slowly move towards a nonzero value after the shape change occurs.
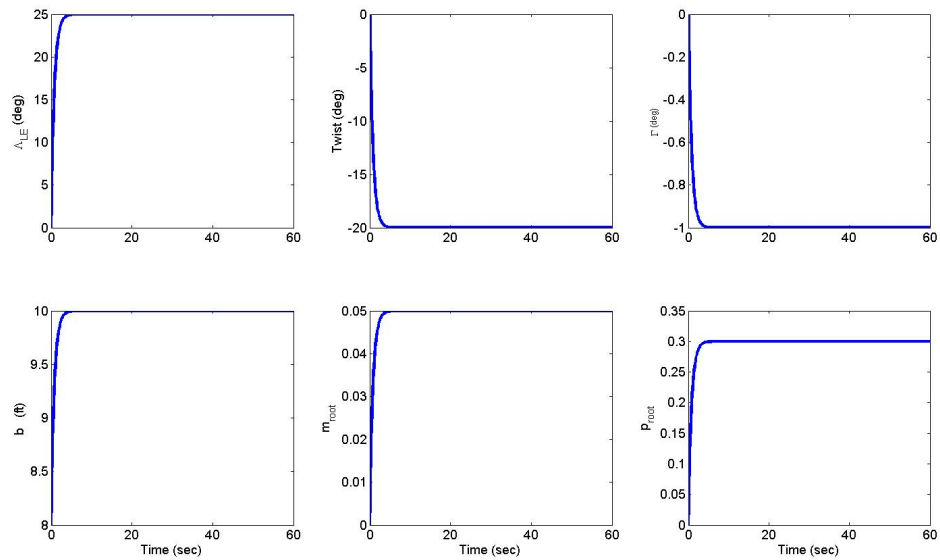
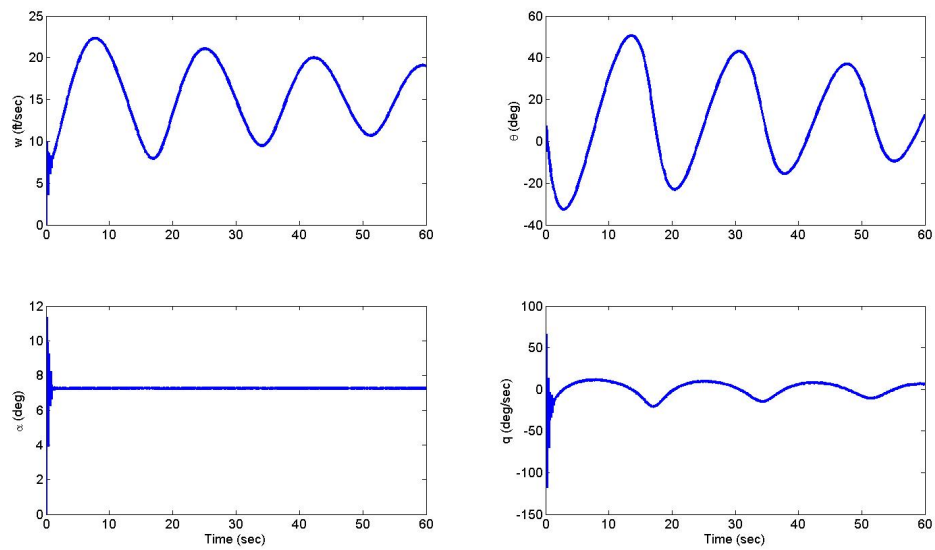Fig. 25. Time History of Morphing Aircraft Shape for Example 3

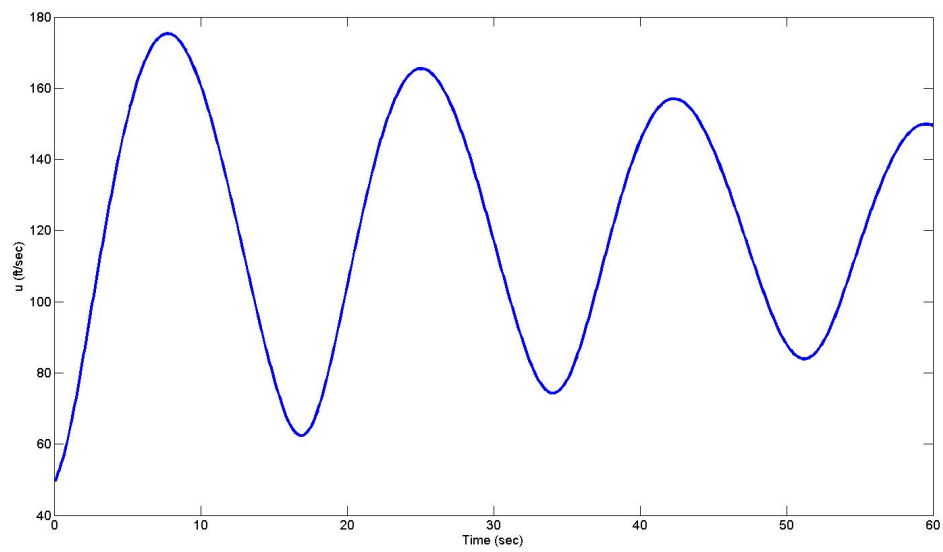Fig. 26. Morphing Aircraft States for Example 3
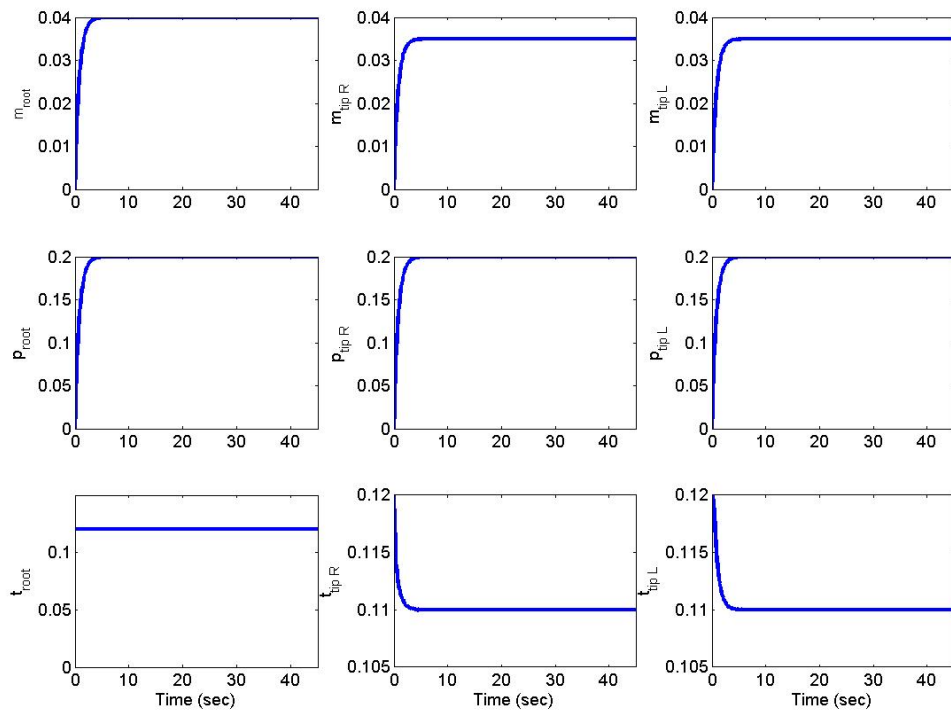
Fig. 27. Time History of u for Example 3

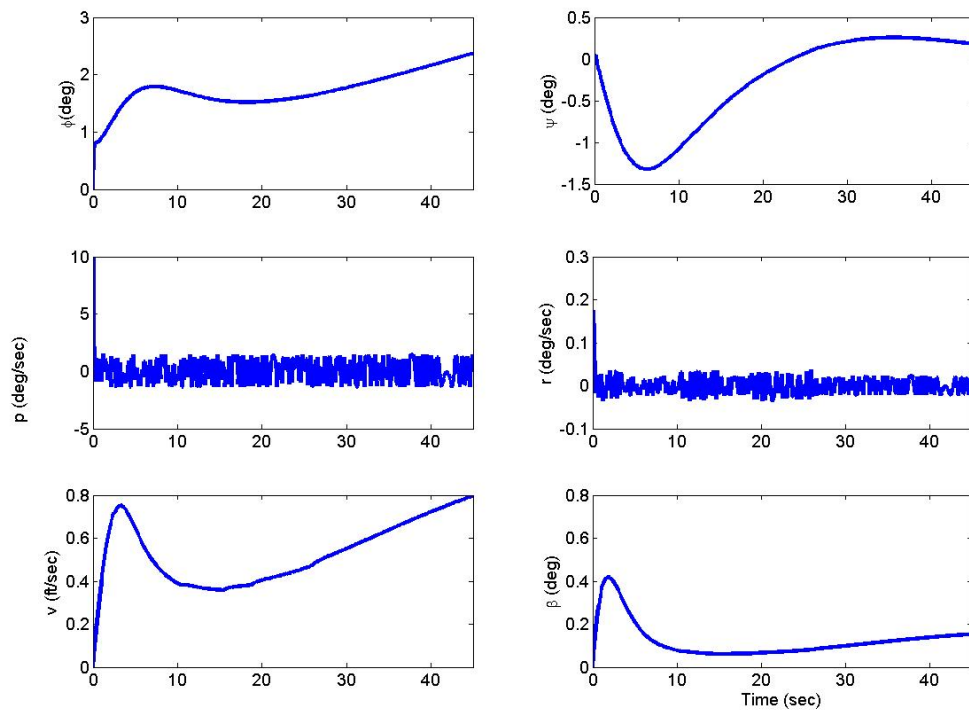Fig. 28. Time History of Morphing Aircraft Shape for Example 4

Fig. 29. Time History of Morphing Aircraft States for Example 4
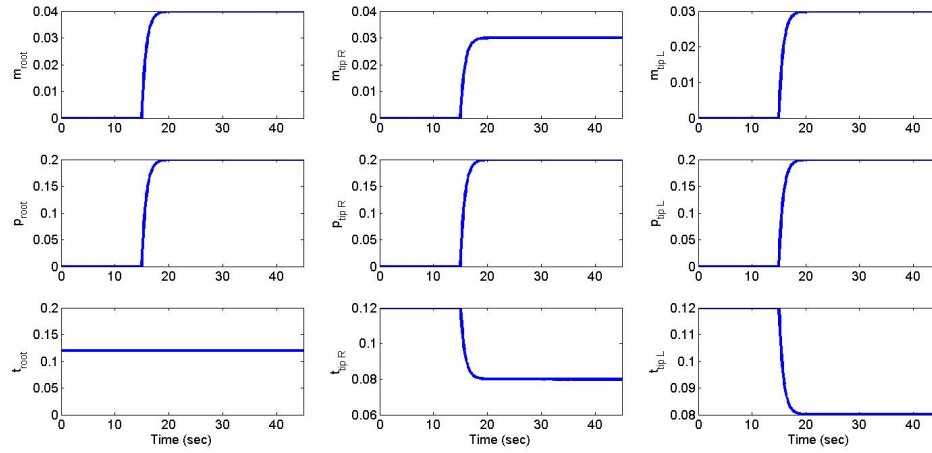
Fig. 30. Time History of Morphing Aircraft Shape for Example 5
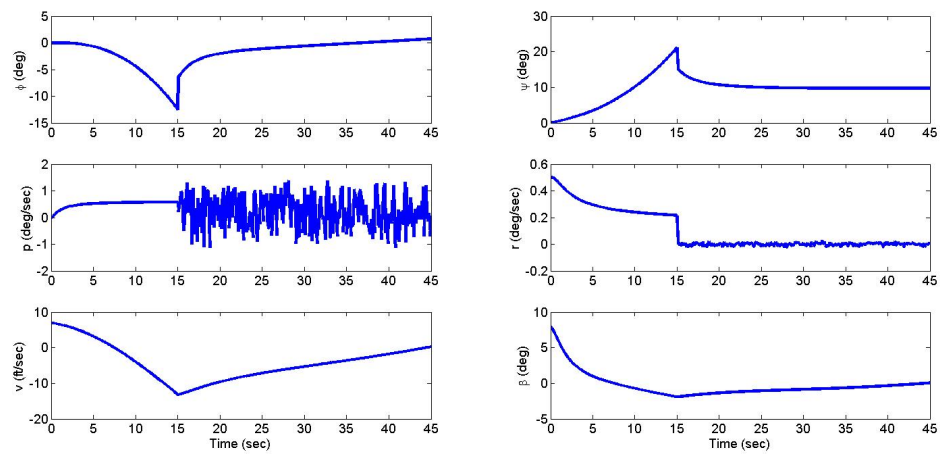

Fig. 31. Time History of Morphing Aircraft States for Example 5

CHAPTER VIII

CONCLUSIONS AND RECOMMENDATIONS

A. Conclusions

This paper develops an aerodynamic model and a dynamic model of a morphing flying wing aircraft. The dynamic model includes accurate aerodynamic forces calculated using the aerodynamic model. The aerodynamic model calculates forces due to large scale shape changing effects. The dynamic model calculates state information for the morphing wing based on the aerodynamic forces from the aerodynamic model. The model allows for multiple shape changing degrees-of-freedom for the wing, including thickness, sweep, dihedral angle, and chord length. Results show the model provides a versatile tool for calculating the aerodynamic forces on the morphing aircraft and the use of these forces to determine the associated states. Two shapes are tested in order to demonstrate the effects of large scale shape changes.

Based on the results presented in this thesis it is concluded that:

1. A computational model for a morphing wing was developed and includes accurate aerodynamic results in incompressible, inviscid flow for basic and complex wing shapes by using a constant strength source-doublet panel code. The dynamical model is able to provide state information based on the aerodynamic forces from the aerodynamic model.

2. The use of cosine spacing in the aerodynamic model reduces the computational time required by approximately 50 per cent. Since the panel method is sensitive to changes in the grid, especially near the leading and trailing edges of the wing, placing more panels in these areas allows for fewer overall panels to be placed on the wing.

3. The dynamic model shows that when the morphing wing does not have any twist or camber, the aircraft is unable to fly at a straight and level configuration. By adding twist and camber to the wing, it is possible place the aircraft at an angle-of-attack which eliminates the aerodynamic pitching moment and provides a constant, positive lift force.

4. A wing with an asymmetric configuration is able to effectively produce rolling and yawing moments which can be used to counter disturbances in rolling and yawing motion.

B. Recommendations

After concluding this research, the following recommendations are made.

1. Add the ability to select reflexed airfoil sections in addition to the NACA 4 Digit series. Since the aircraft is assumed to be a flying wing, having an airfoil with reflexed camber may help with finding a suitable trim state for the aircraft.

2. Investigate the aeroelastic problem. One method for doing this is to develop a structural model of the morphing aircraft and to iterate between the structural model and the aerodynamic model until aeroelastic convergence is shown.

3. In order to make the aerodynamic model more computationally efficient, the aerodynamic model could be used as training data for a neural network. This process was successfully demonstrated on the morphing airfoil model and improved the computational efficiency by one order of magnitude.

4. The addition of viscous effects on the lift and pitching moment should be investigated.

REFERENCES

[1] R.W. Wlezien, CC. Homer, A.R. McGowan, A. Padula, M.A. Scott, R.J. Silcox, and J.O. Simpson, "The Aircraft Morphing Program," *Proceedings of SPIE - The International Society for Optical Engineering*, v 3326, pp. 176-187, 1998

[2] T. M. Seigler, J-S. Bae and D. J. Inman, "Aerodynamic and static aeroelastic characteristics of a variable-span morphing wing," *Journal of Aircraft*, vol. 42, pp. 528-534, Mar.-Apr., 2005.

[3] J. Blondeau, J. Richeson, and D. J. Pines, "Design, development, and testing of a morphing aspect ratio wing using an inflatable telescopic spar," *44th AIAA/ASME/ASCE/AHS Structures, Structural Dynamics, and Materials Conference and Exhibit*, Norfold, VA, 7-10 April 2003, pp. 2883-2893

[4] J. B. Davidson, P. Chwalowski, and B. S. Lazos, "Flight dynamic simulation assessment of a morphable hyper-elliptic cambered span winged configuration," *AIAA Atmospheric Flight Mechanics Conference and Exhibit*, Austin, TX, 11-14 August 2003, AIAA-2003-5301

[5] M. Secanell, A. Suleman, and P. Gamboa, "Design of a morphing airfoil for a light unmanned aerial vehicle using high-fidelity aeodynamic shape optimization," in 46th AIAA/ASME/ASCE/AHS/ASC Structures, Structural Dynamics and Materials Conference and Exhibit, Austin, TX, 18-21 April 2005, AIAA-2005-1891

[6] D. H. Baldelli, D-H. Lee, R. S. Snchez Pea, and B. Cannon, "Modeling and control of an aeroelastic morphing vehicle," *Journal of Guidance, Control, and Dynamics*, vol. 31, no. 6, pp. 1687-1699, Nov.-Dec. 2008.

[7] D. J. Inman, F. H. Gern, and R. K. Kapania, "Structural and aeroelastic modeling of general planform wings with morphing airfoils," *AIAA Journal*, vol. 40, no. 4, pp. 628-637, April 2002.

[8] M. Waszak, A. Wickenheiser, and E. Garcia, "Longitudinal dynamics of a perching aircraft concept," *Journal of Aircraft*, vol. 43, no. 5, pp. 1386-1392, Sept.-Oct. 2006.

[9] M. B. Webb and K. Subbarao, "On the dynamic aeroelastic stability of morphable wing structures," *47th AIAA/ASME/ASCE/AHS/ASC Structures, Structural Dynamics, and Materials Conference and Exhibit*, Newport, RI, 1-4 May 2006, pp. 6374-6386

[10] R. A. Canfield, J. N. Scarlett, and B. Sanders, "Multibody dynamic aeroelastic simulation of a folding wing aircraft," *47th AIAA/ASME/ASCE/AHS/ASC Structures, Structural Dynamics, and Materials Conference and Exhibit*, Newport, RI, 1-4 May 2006, pp. 6398-6407

[11] H. Namgoong, W. A. Crossley, and A. S. Lyrintzis, "Morphing airfoil design for minimum aerodynamic drag and actuation energy including aerodynamic work," *47th AIAA/ASME/ASCE/AHS/ASC Structures, Structural Dynamics, and Materials Conference and Exhibit*, Newport, RI, 1-4 May 2006, pp. 5407-5421

[12] R. K. Nangia and M. E. Palmer, "Morphing ucav wings incorporating in-plane & folded-tips – aerodynamic design studies," *24th Applied Aerodynamics Conference*, San Francisco, CA, 5-8 June 2006, pp. 278-297

[13] J. Bowman, T. Weisshaar, and B. Sanders, "Simulation tool for analyzing complex shape-changing mechanisms in aircraft," *AIAA Modeling and Simulation Technologies Conference and Exhibit*, Keystone, CO, 21-24 August 2006, pp. 1046-1057

[14] J. Valasek, J. Doebbler, M. D. Tandale, and A. J. Meade, "Improved adaptive-reinforcement learning control for morphing unmanned air vehicles," *IEEE Transactions on Systems, Man, and Cybernetics: Part B*, vol. 38, no. 4, pp. 1014-1020, August 2008

[15] J. Bowman, T. Weisshaar, and B. Sanders, "Evaluating the impact of morphing technologies on aircraft performance," *43rd AIAA/ASME/ASCE/AHS/ASC Structures, Structural Dynamics, and Materials Conference*, Denver, CO, 22-25 April 2002, AIAA-2002-1631

[16] T. M. Seigler, D. A. Neal, and D. J. Inman, "Dynamic modeling of large-scale morphing aircraft," *47th AIAA/ASME/ASCE/AHS/ASC Structures, Structural Dynamics, and Materials Conference and Exhibit*, Newport, RI, 1-4 May 2006, pp. 3668-3678

[17] M. Waszak, A. Wickenheiser, and E. Garcia, "Evaluation of bio-inspired morphing concepts with regard to aircraft dynamics and performance," *Proceedings of SPIE-the international society for optical engineering*, 2004, vol 5390, no. 1, pp. 202-211, 2004

[18] J. E. Hubbard Jr, "Dynamic shape control of a morphing airfoil using spatially distributed transducers," *AIAA Journal of Guidance, Control, and Dynamics*, vol. 29, no. 3, pp. 612-616, May-Jun. 2006

[19] K. Boothe, "A design scheme aimed at minimizing actuator and structural loads of a span morphing aircraft," *47th AIAA/ASME/ASCE/AHS/ASC Structures, Structural Dynamics, and Materials Conference and Exhibit*, Newport, RI, 1-4 May 2006 pp. 6418-6427

[20] J. Valasek, M. D. Tandale, and J. Rong, "A reinforcement learning - adaptive control architecture for morphing," *Journal of Aerospace Computing, Information, and Communication*, vol. 2, no. 5, pp. 174-195, April 2005

[21] J. Katz and A. Plotkin, *Low Speed Aerodynamics: 2nd Edition*, New York, NY, Cambridge University Press, 2001, chapter 9, pp. 206-217

[22] J. D. Anderson, *Fundamentals of Aerodynamics*, New York, NY, McGraw-Hill, 2001, chapter 1,2, pp. 22, 180-184

[23] D.H. Allen and W. Haisler, *Introduction to Aerospace Structural Analysis*, John Wiley & Sons, 1985, chapter 4, pp. 146-164

[24] I. Abbot and A. Van Doenhoff, *Theory of Wing Sections*, New York, NY, Dover Publications, 1959, Appendix IV, p. 464

[25] A. Lampton, A. Niksch, and J. Valasek, "Reinforcement learning of morphing airfoils with aerodynamic and structural effects," *Journal of Aerospace Computing, Information, and Communication*, vol. 6, no. 1, pp. 30-50, January 2009

[26] J. Roskam, *Airplane Design Part 1: Preliminary Sizing of Airplanes*, Lawrence, KS, Roskam Aviation and Engineering Corporation, 1989, chapter 3, pp. 118-127

[27] K. Lee, "Development of unmanned aerial vehicle (uav) for wildlife surveillance," M.S. thesis, University of Florida, 2004

[28] J. Moran, *An Introduction to Theoretical and Computational Aerodynamics*, New York, NY, John Wiley & Sons, 1985, chapter 5, pp. 126-128

[29] J. Roskam, *Airplane Flight Dynamics and Automatic Flight Controls*, Lawrence, KS, DARcorporation, 1995, chapter 1, pp. 3-21

VITA

Adam Niksch received his Bachelor of Science in Aerospace Engineering from Texas A&M University in May of 2007. He worked in the industry with Rockwell Collins during the summer of 2007 prior to his entrance into the Aerospace Engineering graduate program at Texas A&M University and graduated with his M.S. in August of 2009.

Mr. Niksch served as the teaching assistant to AERO 421: Dynamics of Aerospace Vehicles for the Fall 2007 and Spring 2008 semesters. Furthermore, he published a journal article with fellow Texas A&M graduate student, Amanda Lampton, and his advisor, Dr. John Valasek, titled: "Reinforcement Learning of Morphing Airfoils with Aerodynamic and Structural Effects" in the *Journal of Aerospace Computing, Information, and Communication*. Currently he has another article in review from the *Journal of Guidance, Navigation, and Control* titled: "Morphing Aircraft Dynamical Model: Longitudinal Shape Changes."

Adam Niksch can be reached at: Aerospace Engineering 701 H R Bright College Station, TX 77843-3141 MS-3141. His email is: adam45611@gmail.com